Hindawi
Journal of Sensors
Volume 2022, Article ID 8111998, 11 pages
https://doi.org/10.1155/2022/8111998

Research Article

Simulation Analysis of Eddy Current Testing Parameters for Surface and Subsurface Defect Detection of Aviation Aluminum Alloy Plate

Weiquan Deng[1], **Jun Bao**[2], **Siqi Luo**[3] and **Xin Xiong**[3]

[1]*Faculty of Mechanical and Electrical Engineering, Kunming University of Science and Technology, Kunming 650500, China*
[2]*Faculty of Civil Aviation and Aeronautics, Kunming University of Science and Technology, Kunming 650500, China*
[3]*Faculty of Information Engineering and Automation, Kunming University of Science and Technology, Kunming 650500, China*

Correspondence should be addressed to Xin Xiong; xinxiong@kust.edu.cn

Received 19 October 2021; Revised 13 December 2021; Accepted 25 February 2022; Published 11 March 2022

Academic Editor: Xue-bo Jin

In the process of eddy current testing (ECT) of surface and subsurface defects of aviation aluminum alloy plates, the setting of parameters is important to the test results. Inappropriate test parameters can cause false detection or even missed detection of defects. To address this problem, the effects of probe type, coil size, and excitation frequency on the accurate identification and quantitative evaluation of surface and subsurface defect detection were studied and analyzed in this study to determine the best testing parameters. The experimental results show that the absolute probe with an outer radius of 3.3 mm has better detection performance for aviation aluminum alloy plate defects. There are different optimal excitation frequency ranges for the surface and subsurface defects. An excitation frequency of 80 kHz to 90 kHz can be used for the detection of unknown defects.

1. Introduction

Aluminum alloy materials are widely used in the manufacture of civil aircraft flaps, skins, and other structural parts owing to their advantages, such as low density, high strength, good processability, and strong corrosion resistance. According to the statistics, in ordinary civil aviation aircraft, the use of aluminum alloy materials exceeds 60% of the total weight of the aircraft. However, owing to the influence of the service environment and long-term high-load operation, various corrosion and fatigue crack defects inevitably occur in aircraft. The existence of defects in aircraft can cause safety hazards to the aircraft structure as well as major safety threats and economic losses. Therefore, it is critical to detect, identify, and accurately quantify the defects in aluminum alloy plates over time.

Among various nondestructive testing (NDT) technologies, eddy current testing (ECT) is the most suitable for the detection of corrosion and fatigue cracks in aircraft aluminum alloy plates owing to its fast detection speed, wide detection range, easy automation, and higher detection performance for surface and subsurface defects of detected objects [1–5]. By combining principal component analysis and k-means classification, Kim et al. conducted feature extraction of a deeper crack in an aircraft to realize defect detection and location [6]. Based on the time-frequency analysis of the pulsed eddy current defect detection signal, combined with k-means clustering and expectation maximization, Hosseini and Lakis realized the automatic detection of the distribution of subsurface defects in each layer of a multilayer aluminum alloy plate structure [7]. He et al. realized the automatic detection of layered defects of an aircraft two-layer aluminum alloy plate structure based on the constructed defect feature and support vector machine classification algorithm and further studied the influence of different lift-off distances on the detection results [8]. Li et al. studied the subsurface defect detection of aluminum alloy plates based on pulse-modulated eddy currents, which improved the detection performance of subsurface defects [9]. For the detection of subsurface defects in aluminum

alloy plates, Perumal et al. conducted a simulation analysis from multiple excitation frequencies, and combined with the optimization of excitation frequency, the depth of different subsurface defects can be located [10]. Yan et al. used the improved Canny algorithm to identify the edge of the defect ECT image of aluminum alloy materials, which improved the accuracy of corrosion edge detection under coating [11]. Considering the influence of edge effects on defect detection, Xie et al. conducted finite element simulation from the design of probe parameters to improve the ability of edge defect detection [12]. In addition, for defect detection, some studies have been conducted on the combination of the probe type and defect scanning method.

However, in the existing research on defect detection of aluminum alloy plate materials, most of the studies are based on single detection parameter optimization and detection signal processing algorithms for defect detection and quantitative analysis [13–16], thus insufficient accuracy of subsurface defect detection and defect edge extraction. Starting from the detection parameters, in this study, we analyze the effects of probe type, coil size, and excitation frequency on the surface and subsurface defect detection of aviation aluminum alloy plates and construct a finite element model to optimize the detection parameters. The rest of this paper is organized as follows: First, the theoretical method of probe coil design is analyzed in Section 2. Second, the finite element model of the ECT is constructed, and several testing parameters are set in Section 3. Next, the simulation results are analyzed in detail in Section 4. Finally, conclusions and further research are outlined in Section 5.

2. Theoretical Method

ECT is an NDT method based on the change in the electromagnetic properties of the tested conductor to analyze its properties and defects. This method is based on electromagnetism theory. When a current of a certain frequency flows into the excitation coil, under the action of electromagnetic induction, the induced eddy current is generated in the detected conductor. Furthermore, the induced eddy current generates a magnetic field and reacts on the test coil, thus affecting the voltage and current of the coil.

The ECT coil is composed of multiple turns of metal enameled wire; thus, the coil itself has inductance. In addition, there is resistance between the winding enameled wire, as well as a coupling capacitor between each turn of the coil. In actual detection and calculation, the capacitance distributed between each turn of the coil is usually ignored. The coil can be expressed as a series circuit of inductance L_1 and resistance R_1, and the complex impedance of the coil itself can be expressed as

$$Z_1 = R_1 + j\omega L_1. \tag{1}$$

Under the action of the induced eddy current excited by the excitation coil, the conductor can be expressed as a secondary circuit composed of inductance and resistance in series. The complex impedance of the coil is affected by the equivalent impedance Z_z of the conductor.

$$Z_z = R_z + j\omega L_z = \frac{\omega^2 M^2}{{R_2}^2 + \omega^2 {L_2}^2} R_2 + j\omega \frac{\omega^2 M^2}{{R_2}^2 + \omega^2 {L_2}^2} L_2. \tag{2}$$

L_2 and R_2 are the equivalent inductance and resistance of the conductor under test, M is the mutual inductance between the coil and the conductor, and M can be expressed as

$$M = k(l)\sqrt{L_1 L_2}. \tag{3}$$

$k(l)$ is the coupling coefficient, which is related to the lift-off distance between the coil and conductor. The change in the electromagnetic properties of the conductor affects its equivalent impedance Z_z and, consequently, affects the complex impedance of the detection coil. The conductivity, permeability, defect, and thickness (sheet) of the conductor can be obtained by collecting and analyzing the impedance signal of the detection coil.

The design of the ECT probe coil should follow the appropriate inductance value, resistance value, and higher Q value (i.e., quality factor, $Q = \omega L/R$). For a multiturn coil, without considering the influence of the capacitance between the turns of the enameled wire, the inductance L is proportional to the square of the number of turns N of the coil, that is,

$$L \propto N^2 = \frac{(r_2 - r_1)^2 h^2}{d^4}. \tag{4}$$

r_2, r_1, and h are the outer radius, inner radius, and height of the coil, respectively, and d is the diameter of the enameled wire.

The resistance of the coil itself can be calculated according to the following formula:

$$R = \rho \frac{l}{S} = 4\rho \frac{\pi\left({r_2}^2 - {r_1}^2\right)h}{d^4}. \tag{5}$$

Combining Equations (3) and (5), the quality factor Q of the coil can be expressed as follows:

$$\mathrm{Q} = \frac{\omega L}{R} \propto \frac{\omega h}{\rho} \cdot \frac{r_2 - r_1}{r_2 + r_1}. \tag{6}$$

It can be observed from the above equation that when the wire of the coil is determined, Q is determined by the excitation frequency and coil size. In the defect detection process, if the coil is significantly small, the excitation current of the coil must be reduced accordingly. Moreover, if the excitation current is significantly small, the detected induction signal reduces, which further causes the defect signal to be submerged in noise, thus the inability to obtain an effective detection signal. However, if the coil radius is increased, a coil that is considerably large creates a difference between the detected defect edge and the actual defect edge; thus, defect edge detection becomes difficult.

For the ECT of surface and subsurface defects of aviation aluminum alloy plates, in this study, we simulated and

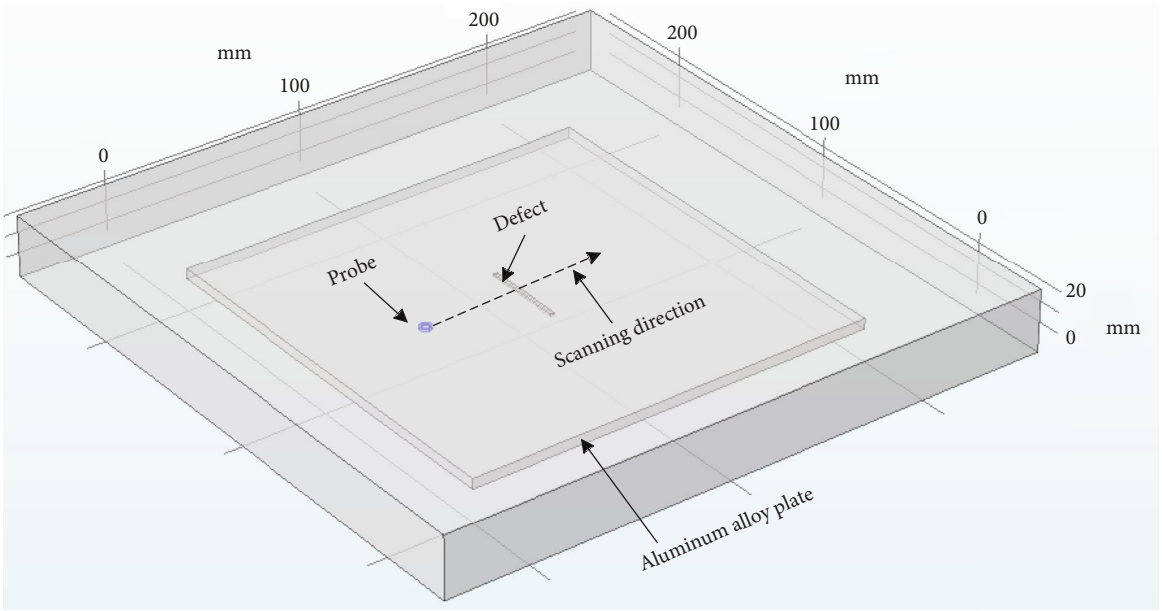

Figure 1: Finite element simulation model of ECT.

Table 1: Electromagnetic properties of the simulation model.

Material	Electromagnetic properties	
	Conductivity (MS/m)	Relative permeability
6000 series aluminum alloys specimen	26	1
Probe coil made of copper	58	0.99
Vacuum computing region	0	1

optimized the probe type, coil radius, and excitation frequency to improve the accuracy of defect detection and defect edge recognition.

3. Simulation Experiment Modeling

To accurately analyze the effects of probe type, coil size, and excitation frequency on the accuracy of surface and subsurface defect detection and edge recognition of aviation aluminum alloy plates, a finite element model of ECT based on COMSOL multiphysical field simulation platform was constructed in this study, as shown in Figure 1. The simulation model included an aluminum alloy specimen, eddy current probe, and vacuum domain. In this model, different parameters, such as the probe type, coil size, and excitation frequency, were simulated and calculated. The depth and position of the defects in the specimen and the size of the coil were set according to different research contents.

The specimen chosen for this study was a 6000 series aluminum alloy plate with a thickness of 5 mm that contains defects of different sizes. The coil was composed of copper enameled wire and placed above the specimen. The distance between the coil and the specimen was set to 1 mm. The electromagnetic properties of simulation model materials are shown in Table 1.

Before the simulation calculation, the model should be meshed and divided into multiple elements. It is necessary to consider the accuracy and efficiency of calculation simultaneously when meshing. The smaller the element is, the higher the calculation accuracy will be, and the calculation time will increase accordingly. Considering that the inspection object constructed was an aluminum alloy thin plate, a smaller mesh division did not significantly increase the calculation time; thus, extremely fine mesh generation was adopted in this study, as shown in Figure 2.

Based on meshing, the combination of parametric scanning and frequency domain analysis was used for simulation calculation. The scanning path of defects in the simulation process is shown in Figure 1. Assuming the defect as the center, the left and right sides were both 25 mm for scanning of the defect, and the scanning step is 0.5 mm. After the simulation solution, the coil impedance at different positions and frequencies was obtained.

3.1. Simulation of Coil Structure. In the process of fatigue crack detection and analysis of aircraft aluminum alloy plates, different probe types have an impact on the accuracy of defect detection and edge recognition. The common eddy current probe selection includes the absolute and differential types. As shown in Figure 3, the excitation and receiving coils are the same as those in the absolute probe. In Figure 4, the excitation of the differential probe consists of two inversely connected coils, and the receiving coil is placed between the two excitation coils (differential excitation).

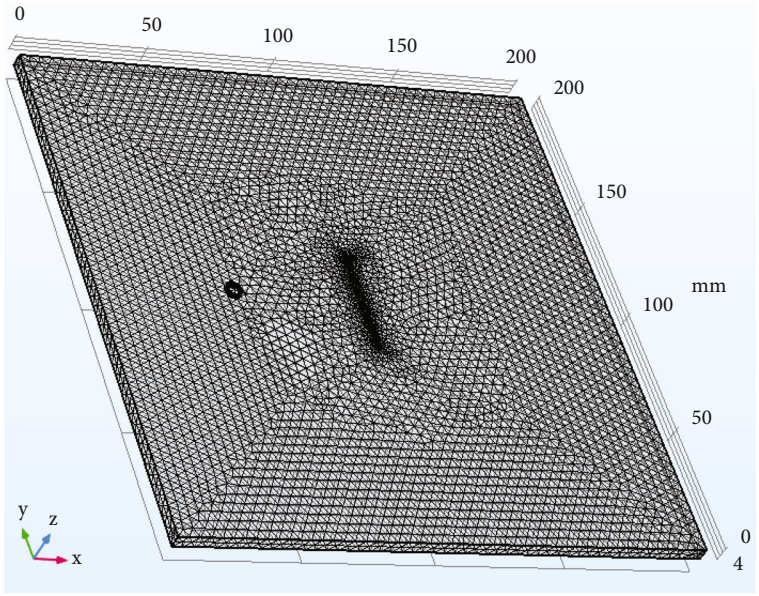

Figure 2: Meshing of the simulation model.

Another form of differential probe is that the receiving coil is completed by two reverse-connected coils, and the excitation coil is placed in the middle of the receiving coil, that is, differential reception. Compared with the differential receiving probe, the differential excitation probe exhibited stronger anti-interference. Therefore, the differential excitation probe was used for the simulation experiment analysis of defect detection in this study.

According to Equation (6), it can be observed that the quality factor is determined by the inductance and resistance of the coil, which can be further transformed into the relationship with the coil size. Considering that the detection object was the defect of the aluminum alloy plate, the change in the coil height did not affect the detection of the defect edge. The quality factor was further simplified as the relationship between the inner and outer diameters of the coil. The inner and outer radius ranges were 1–4 mm and 2–5 mm, respectively, and the corresponding coil quality factor was calculated. The results are shown in Figure 5.

From the simplified calculation results, the quality factor was affected by the outer radius. The larger the outer radius, the higher the quality factor. The quality factor was not affected by the change of coil inner radius. When the ratio of inner radius to outer radius was less than 0.6, it can be considered to be in an appropriate range. However, in the process of defect detection, we should be able to accurately identify the existence of defects, as well as accurately identify the edge of defects from the detection signal, in order to make quantitative analysis of defects. Therefore, the larger the outer diameter of the coil used for defect detection is not the better.

In the defect scanning shown in Figure 1, it is necessary to accurately identify the defect and its edge information from the detection signal. To study the influence of different probe selections on defect edge recognition, 2 mm and 20 mm defects with different widths were set, and the simulation parameters are listed in Table 2.

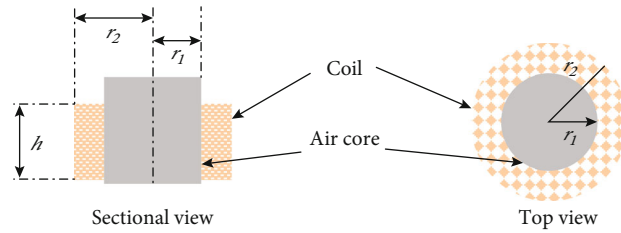

Figure 3: Schematic diagram of absolute probe.

To study the coil size of probe suitable for crack defect detection of aviation aluminum alloy plate, the scanning experiments of coils with different sizes were carried out on the simulation model constructed in Figure 1. The experimental parameters are shown in Table 3; seven coil outer radii of different sizes are set. When the inner radius of the coil is 0.3~0.6 times of the outer radius, the appropriate quality factor Q of the coil can be guaranteed [17].

3.2. Simulation of Excitation Frequency. Owing to the skin effect of the eddy current, the penetration depth of the eddy current decreases sharply with an increase in the excitation frequency. If the excitation frequency is significantly small, the resolution of the ECT signal to defects becomes insufficient, making it difficult to accurately identify defects. If the excitation frequency is considerably large, deeper defects cannot be detected, and an excessive excitation frequency causes the eddy current signal to be more susceptible to noise interference. Therefore, it is necessary to determine a more suitable excitation frequency for the defect detection of aviation aluminum alloy plates.

Four surface defects and subsurface defects with different depths were constructed in an aviation aluminum alloy plate, and the defects were detected by frequency sweeping.

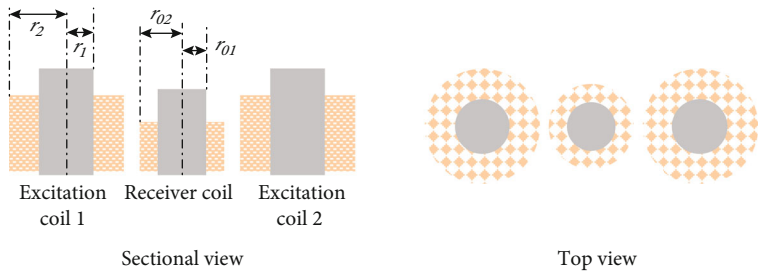

Figure 4: Schematic diagram of differential probe.

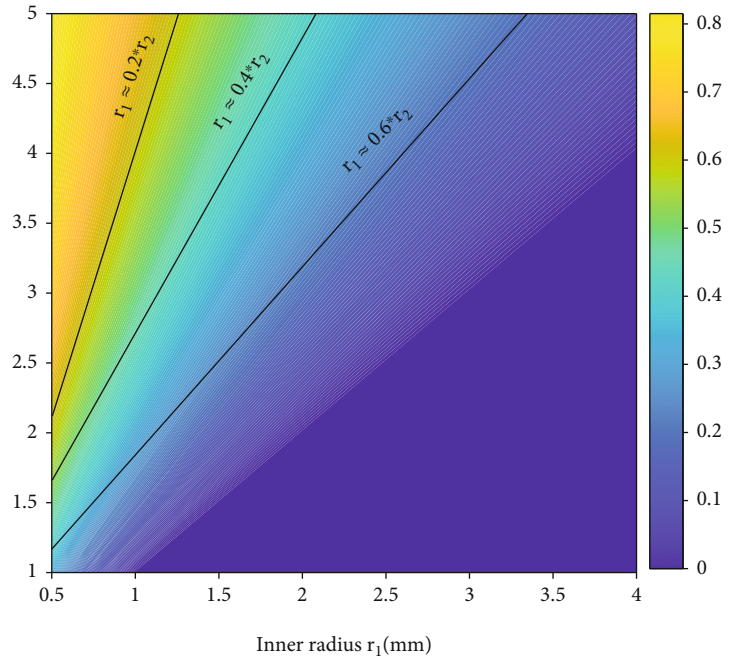

Figure 5: The relationship between coil quality factor and inner and outer radius.

Table 2: Parameters of absolute and differential probes for scanning defects.

Excitation frequency (kHz)	Excitation current (mA)	Coil parameters				Defect information (length × width × depth (mm))	
		Turns	r_1, r_{01} (mm)	r_2, r_{02} (mm)	h (mm)	#1	#2
100	50	300	2	3	1	40 × 2 × 1	40 × 20 × 1

The defects with different sizes are shown in Figure 6, and the simulation parameters are shown in Table 4.

4. Analysis of Experimental Results

4.1. Simulation Analysis of Coil Structure. According to the simulation parameters set in Table 2, the scanning results of different probe types for defect detection based on the constructed simulation model are shown in Figures 7 and 8, respectively. The horizontal and vertical axes represent the position and impedance value of the probe, respectively, and 0 in the horizontal axis represents the defect center. From the scanning results of the absolute probe on the defect in Figure 7, the signal in the entire defect area can be clearly identified, and the defect edge information can be accurately reflected in the scanned signal. However, in the scanning results of the differential probe for defects shown in Figure 8, the eddy current signal has multiple upward and downward trends in both defect areas, and the defect area and the edge information of the defect cannot be clearly identified from the scanned signal. It can be observed that the absolute probe is suitable for defect detection and quantitative analysis.

According to the above analysis, the detection signal is required to meet easy defect identification and edge detection simultaneously during defect detection, that is, accurate defect classification and quantitative analysis. For the defect detection signal obtained by simulation, the impedance difference Z_{diff} between the detection coil at the defect and

Table 3: Influence of different outer radius of coil on defect detection.

r_2 (mm)	r_1 (mm)	Excitation frequency (kHz)	Excitation current (mA)	Defect information (length × width × depth (mm))
2, 2.5, 3, 3.5, 4, 4.5, 5	$0.3 \sim 0.6 \times r_2$	100	50	$40 \times 1 \times 1$

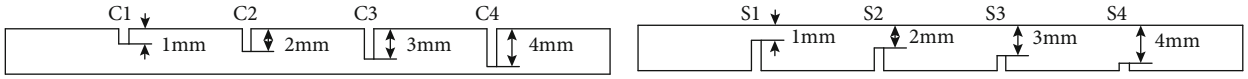

(a) Surface defects (b) Subsurface defects

Figure 6: Schematic diagram of specimen defects.

Table 4: Influence of excitation frequency on defect detection.

Frequency range (kHz)	Step (kHz)	Depth of defect (mm)		r_2 (mm)	r_1 (mm)
		Surface defects	Subsurface defects		
10~1000	10	1, 2, 3, and 4	1, 2, 3, and 4	3	1.5

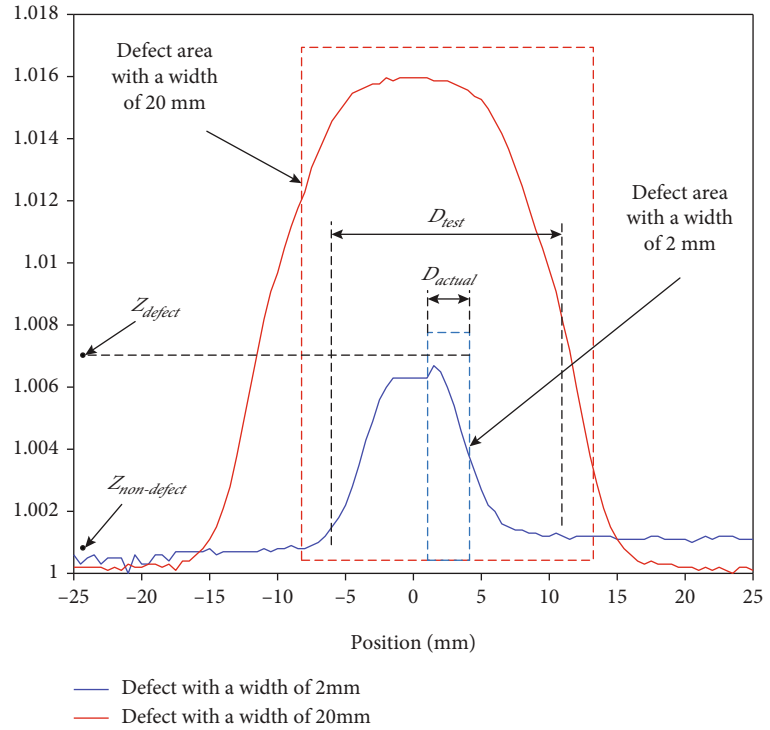

Figure 7: Scanning signal of absolute probe to defect.

nondefect and the proportion P_{ratio} of the scanning points of the actual defect area to the defect area determined by the scanning signal are calculated. According to the notes in Figure 7, Z_{diff} and R_{ratio} are calculated as follows:

$$Z_{diff} = Z_{defect} - Z_{nondefect},$$
$$P_{ratio} = \frac{D_{actual}}{D_{test}} \times 100. \quad (7)$$

The simulation solution was conducted according to the parameters set in Table 3, and Z_{diff} and P_{ratio} were calculated for the solution results of different outer radii. The simulation and calculation results are shown in Figure 9.

As shown in Figure 9, with the increase of the outer radius of the coil, the impedance difference Z_{diff} also gradually increases; that is, a larger coil radius is conducive to the detection of defects. However, the proportion P_{ratio} decreases with the increase of the coil radius; that is, the larger the coil

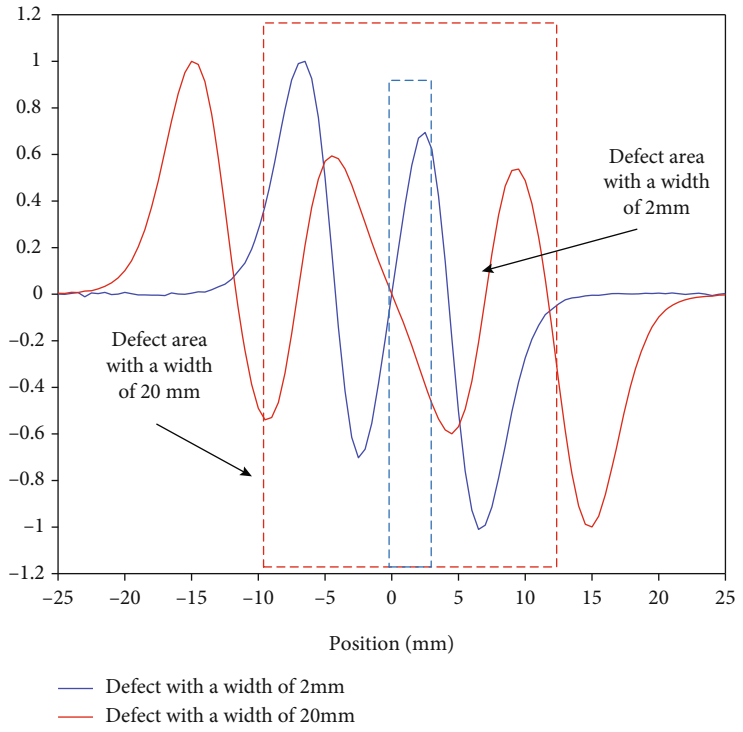

Figure 8: Scanning signal of differential probe to defect.

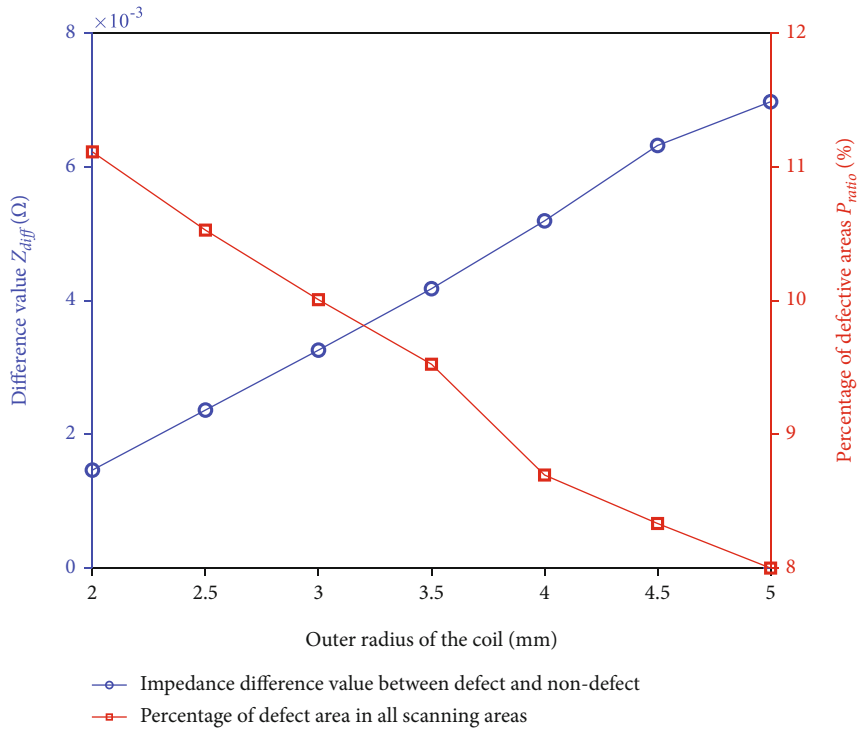

Figure 9: Simulation of coils with different sizes.

radius, the more difficult it is to identify the edge information of the defect from the detection signal. From the comprehensive analysis of the simulation results, when the outer radius of the coil is 3.3 mm, both defect detection and edge recognition can achieve higher accuracy.

4.2. Simulation Analysis of Excitation Frequency. According to the simulation parameters set in Table 4, the parametric scanning detection is conducted for surface and subsurface defects, as well as the impedance difference Z_{diff} between defect and nondefect is calculated using the constructed

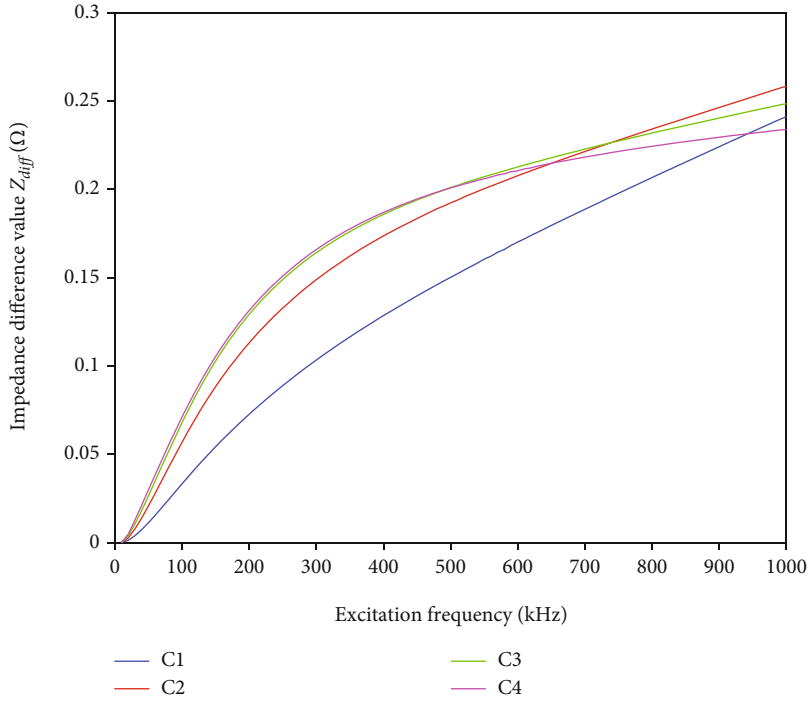

Figure 10: Influence of excitation frequency on surface defect detection.

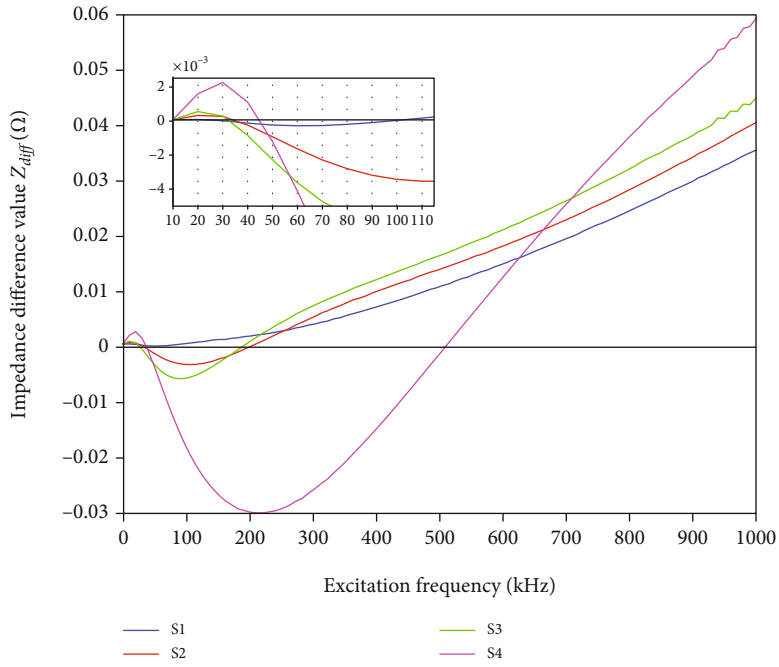

Figure 11: Influence of excitation frequency on subsurface defect detection.

simulation model. The detection results of surface defects and subsurface defects are shown in Figures 10 and 11, respectively.

In the surface defect simulation results shown in Figure 10, for defects with different depths, the impedance difference Z_{diff} increases with an increase in the excitation frequency. However, with the increase in surface defect depth, the impedance difference Z_{diff} tends to be stable at higher frequencies, and there is no increasing trend. The deeper the defect, the earlier it shows a stable trend.

In the simulation results of subsurface defects shown in Figure 11, the change in impedance difference Z_{diff} is complex. Within a certain excitation frequency range, the impedance value at the defect is greater than that at the nondefect; that is, the impedance difference Z_{diff} is positive. With an increase in the excitation frequency, the

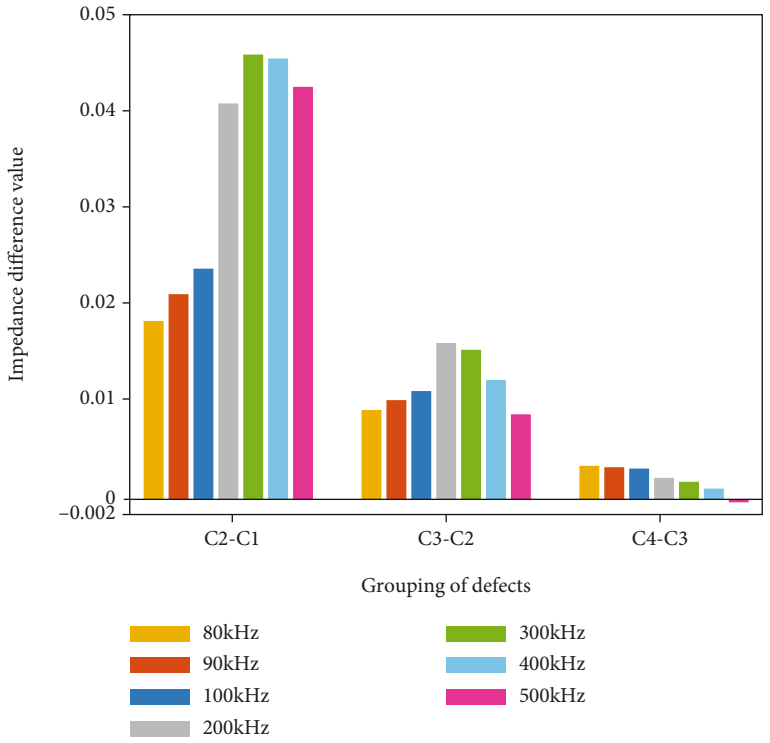

Figure 12: Influence of different excitation frequencies on impedance difference of surface defects at different depths.

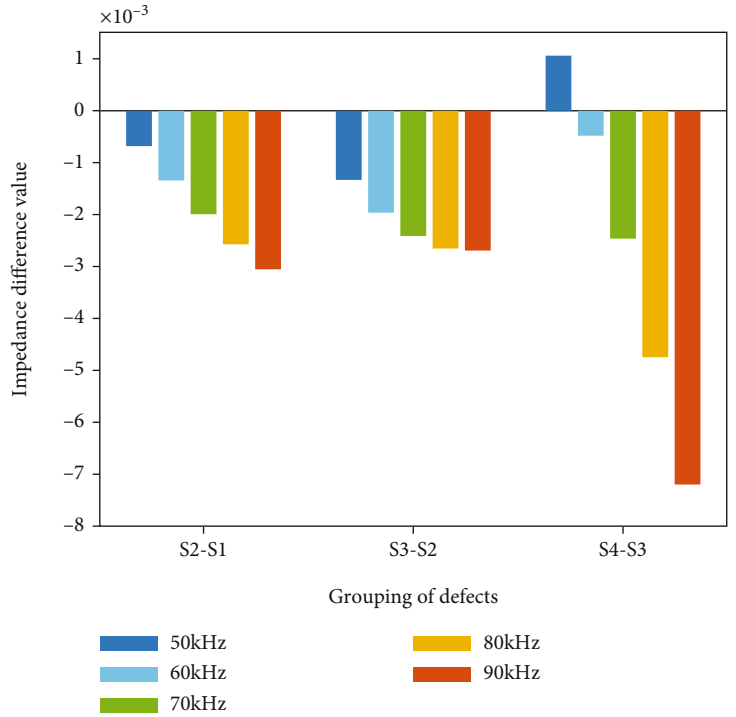

Figure 13: Influence of different excitation frequencies on impedance difference of subsurface defects with different depths.

impedance difference gradually decreases. The impedance difference Z_{diff} of defects S1–S4 is 0 at different excitation frequencies; that is, the impedance value at the defect is equal to that at the nondefect. When the excitation frequency is increased, the impedance value at the defect is less than that of the nondefect, and the impedance difference Z_{diff} is negative.

According to the previous analysis, in the ECT process, the greater the difference in signals between different defects, the more conducive to the identification, classification, and

Table 5: Simulation and analysis results of parameter setting.

Parameter		Value
Probe type		Absolute probe
Outer radius of coil (r_2)		3.3 mm
Inner radius of coil (r_1)		$\leq 0.6 \times r_2$
Excitation frequency	Surface defect	80~400 kHz
	Subsurface defect	60~90 kHz

quantitative analysis of defects. To further determine the optimal excitation frequency for defect detection of aviation aluminum alloy plates, the difference in impedance between adjacent defects was calculated. The calculated differences between surface defects and subsurface defects are shown in Figures 12 and 13, respectively.

In the statistics of impedance difference of surface defects shown in Figure 12, the impedance difference of adjacent defects under six frequency excitations of 80 kHz, 90 kHz, 100 kHz, 200 kHz, 300 kHz, 400 kHz, and 500 kHz was analyzed. It can be observed that as the defect depth increases, the impedance difference corresponding to each excitation frequency decreases, and the impedance value of deeper defects is less than that of shallow defects at higher excitation frequencies. Combined with the analysis of Figures 10 and 12, for the surface defects of the aviation aluminum alloy plate, the excitation frequency can achieve an accurate detection effect in the range of 80 kHz to 400 kHz.

Similarly, in order to accurately classify, identify, and quantitatively analyze a variety of subsurface defects, the impedance difference of adjacent defects was analyzed from six excitation frequencies of 50 kHz, 60 kHz, 70 kHz, 80 kHz, and 90 kHz, as shown in Figure 13. In shallow subsurface defects, such as 1 mm, 2 mm, and 3 mm deep defects, the impedance difference increases with an increase in the excitation frequency. However, when the defect depth is 3–4 mm and the excitation frequency is 50 kHz, the impedance value of shallow defects is greater than that of deep defects, which further causes difficulty in defect classification and identification as well as quantitative evaluation.

Through comprehensive analysis of the optimal excitation frequency of defect detection shown in Figures 12 and 13, surface defects and subsurface defects can achieve good detection results in the excitation frequency range of 80 kHz~90 kHz. In the actual defect detection process, the 80 kHz~90 kHz excitation frequency can be used to preliminarily judge the defect type and then adjust the excitation frequency for different types of defects to collect defect signals to realize accurate identification, classification, and quantitative analysis of defects. The simulation analysis results of the ECT parameters for aviation aluminum alloy plate defects are listed in Table 5.

When ECT technology was used for defect detection of aviation aluminum alloy plates, an absolute probe with an outer radius of 3.3 mm was used as the probe, and the inner radius of the coil was less than 0.6 times its outer radius. At this time, the probe can simultaneously meet the accuracy of defect detection and edge recognition. In addition, for the setting of the excitation frequency during defect detection, the frequency adaptation ranges of surface and subsurface defects are 80~400 kHz and 60~90 kHz, respectively. An excitation frequency of 80~90 kHz can be used for detection to realize accurate detection, identification, and quantitative analysis of defects.

5. Conclusion

To address the problem of surface and subsurface defect detection as well as quantitative analysis of aviation aluminum alloy plates, a comprehensive simulation optimization analysis was conducted using probe type, coil size, and excitation frequency. Compared with the differential probe, the absolute probe has better defect identifiability and defect edge detection ability. Meanwhile, when the outer radius is 3.3 mm, the absolute probe can further improve the defect detection ability and defect edge detection accuracy. In addition, for the excitation frequency range of 80 kHz to 90 kHz, the detection ability for unknown defects was further improved. The optimization analysis of the parameter settings of defect detection through simulation modeling can guide the probe design and excitation frequency setting in the actual detection process. In addition, it can promote the application of computer-aided design and optimization in the eddy current detection of aviation aluminum alloy defects. The future work of this paper will continue from two aspects: First, we will combine simulation signals and intelligent algorithms to further improve the accuracy of defect edge recognition; thereafter, we will verify and improve it with the measured signal. Second, we will combine the simulation model and the measured signal to study the influence of different scanning paths on defect detection.

Data Availability

The [data.rar] data used to support the findings of this study have been deposited in the Aliyun Server repository (http://120.76.226.240/KH_AnCore/data.rar), and other researchers can download original data from this URL.

Conflicts of Interest

The authors declare that there is no conflict of interests regarding the publication of this paper.

Acknowledgments

This work is supported by the Applied Basic Research Programs of Science and Technology Commission Foundation of Yunnan Province under Grant 2019FB081.

References

[1] A. Sophian, G. Y. Tian, D. Taylor, and J. Rudlin, "Design of a pulsed eddy current sensor for detection of defects in aircraft lap-joints," *Sensors and Actuators A: Physical*, vol. 101, no. 1-2, pp. 92–98, 2002.

[2] T. Chen, G. Y. Tian, A. Sophian, and P. W. Que, "Feature extraction and selection for defect classification of pulsed eddy current Ndt," *Ndt & E International*, vol. 41, no. 6, pp. 467–476, 2008.

[3] M. Morozov, G. Y. Tian, and P. J. Withers, "The pulsed eddy current response to applied loading of various aluminium alloys," *NDT & E International*, vol. 43, no. 6, pp. 493–500, 2010.

[4] X. Chen, D. Hou, L. Zhao, P. Huang, and G. Zhang, "Study on defect classification in multi-layer structures based on fisher linear discriminate analysis by using pulsed eddy current technique," *NDT & E International*, vol. 67, pp. 46–54, 2014.

[5] W. Deng, B. Ye, J. Bao, G. Huang, and J. Wu, "Classification and quantitative evaluation of eddy current based on kernel-Pca and elm for defects in metal component," *Metals*, vol. 9, no. 2, p. 155, 2019.

[6] J. Kim, G. Yang, L. Udpa, and S. Udpa, "Classification of pulsed eddy current Gmr data on aircraft structures," *Ndt & E International*, vol. 43, no. 2, pp. 141–144, 2010.

[7] S. Hosseini and A. A. Lakis, "Application of time–frequency analysis for automatic hidden corrosion detection in a multi-layer aluminum structure using pulsed eddy current," *Ndt & E International*, vol. 47, pp. 70–79, 2012.

[8] Y. He, M. Pan, D. Chen, and F. Luo, "Pec defect automated classification in aircraft multi-ply structures with interlayer gaps and lift-offs," *NDT & E International*, vol. 53, pp. 39–46, 2013.

[9] Y. Li, B. Yan, D. Li, H. Jing, Y. Li, and Z. Chen, "Pulse-modulation eddy current inspection of subsurface corrosion in conductive structures," *Ndt & E International*, vol. 79, pp. 142–149, 2016.

[10] M. R. Perumal, K. Balasubramaniam, and K. Arunachalam, "Study of the choice of excitation frequency for sub surface defect detection in electrically thick conducting specimen using eddy current testing," *Journal of Nondestructive Evaluation*, vol. 37, no. 4, p. 70, 2018.

[11] B. Yan, Y. Li, S. Ren, I. M. Zainal Abidin, Z. Chen, and Y. Wang, "Recognition and evaluation of corrosion profile via pulse-modulation eddy current inspection in conjunction with improved Canny algorithm," *NDT & E International*, vol. 106, pp. 18–28, 2019.

[12] Y. Xie, J. Li, Y. Tao, S. Wang, W. Yin, and L. Xu, "Edge effect analysis and edge defect detection of titanium alloy based on eddy current testing," *Applied Sciences*, vol. 10, no. 24, p. 8796, 2020.

[13] Y. He, F. Luo, M. Pan, X. Hu, J. Gao, and B. Liu, "Defect classification based on rectangular pulsed eddy current sensor in different directions," *Sensors and Actuators A: Physical*, vol. 157, no. 1, pp. 26–31, 2010.

[14] J. Wu, D. Zhou, and J. Wang, "Surface crack detection for carbon fiber reinforced plastic materials using pulsed eddy current based on rectangular differential probe," *Journal of Sensors*, vol. 2014, 8 pages, 2014.

[15] K. Zhang, Y. He, and Z. Dong, "Pulsed eddy current nondestructive testing for defect evaluation and imaging of automotive lightweight alloy materials," *Journal of Sensors*, vol. 2018, 11 pages, 2018.

[16] D. J. Pasadas, H. G. Ramos, B. Feng, P. Baskaran, and A. L. Ribeiro, "Defect classification with Svm and wideband excitation in multilayer aluminum plates," *IEEE Transactions on Instrumentation and Measurement*, vol. 69, no. 1, pp. 241–248, 2020.

[17] H. Wang, W. Li, and Z. Feng, "Noncontact thickness measurement of metal films using eddy-current sensors immune to distance variation," *IEEE Transactions on Instrumentation and Measurement*, vol. 64, no. 9, pp. 2557–2564, 2015.